Biochimie 97 (2014) 152–162

Contents lists available at ScienceDirect

Biochimie

journal homepage: www.elsevier.com/locate/biochi

Research paper

Exploring unsymmetrical dyads as efficient inhibitors against the insect β-*N*-acetyl-D-hexosaminidase OfHex2

Qi Chen [a], Peng Guo [b], Lin Xu [b], Tian Liu [a], Xuhong Qian [b,**], Qing Yang [a,*]

[a] School of Life Science and Biotechnology, Dalian University of Technology, No.2 Linggong Road, Dalian, Liaoning 116024, China
[b] State Key Laboratory of Bioreactor Engineering and Shanghai Key Laboratory of Chemical Biology, School of Pharmacy, East China University of Science and Technology, Shanghai 200237, China

ARTICLE INFO

Article history:
Received 23 July 2013
Accepted 9 October 2013
Available online 17 October 2013

Keywords:
β-*N*-Acetyl-D-hexosaminidase
Enzyme inhibitors
Molecular docking
Naphthalimide
Tryptophan fluorescence titration

ABSTRACT

The GH20 β-*N*-acetyl-D-hexosaminidase OfHex2 from the insect *Ostrinia furnacalis* (Guenée) is a target potential for eco-friendly pesticide development. Although carbohydrate-based inhibitors against β-*N*-acetyl-D-hexosaminidases are widely studied, highly efficient, non-carbohydrate inhibitors are more attractive due to low cost and readily synthetic manner. Based on molecular modeling analysis of the catalytic domain of OfHex2, a series of novel naphthalimide-scaffold conjugated with a small aromatic moiety by an alkylamine spacer linker were designed and evaluated as efficiently competitive inhibitors against OfHex2. The most potent one containing naphthalimide and phenyl groups spanning by an *N*-alkylamine linker has a K_i value of 0.37 μM, which is 6 fold lower than that of **M-31850**, the most potent non-carbohydrate inhibitor ever reported. The straightforward synthetic manners as well as the presumed binding model in this paper could be advantageous for further structural optimization for developing inhibitors against GH20 β-*N*-acetyl-D-hexosaminidases.

1. Introduction

Glycoside hydrolase family 20 (GH20) β-*N*-acetyl-D-hexosaminidases (EC 3.2.1.52) catalyze the hydrolysis of *N*-glycans by liberating *N*-acetyl-D-glucosamine (GlcNAc) or *N*-acetyl-D-galactosamine (GalNAc) from non-reducing ends. It plays important roles in the degradation of lysosomal or spermatozoa plasma glycoconjugates and the degradation of chitin [1].

OfHex2 is a presumed insect lysosomal β-*N*-acetyl-D-hexosaminidase from the destructive pest *Ostrinia furnacalis* (Guenée) [2]. It has been proved to play an important role in the development of larval abdomen, pupal wing and adult appendages by means of RNAi [3]. These properties distinguishes OfHex2 from the insect chitinolytic enzymes, OfHex1, the homolog that functions in chitin degradation during insect molting [2,4,5]. Besides, the comparison between substrate spectrums of OfHex2 and its human homolog HsHex indicates insect OfHex2 is quite different from HsHex. Thus, OfHex2 would be an insect-specific target potential, and diminishing or decreasing the activity of OfHex2 is perhaps an efficient and eco-friendly path for pest control.

A number of inhibitors against β-*N*-acetyl-D-hexosaminidases have been reported during recent years [6–11]. Among them, carbohydrate derivatives are most potent ones. Fig. 1 lists seven structures with high inhibitory activities. NAG-thazoline (NGT) is the analog of the transient oxazoline intermediate with a K_i value of 0.07 μM against human β-*N*-acetyl-D-hexosaminidase B (HsHexB) and a K_i value of 0.06 μM against a bacterial GH20 β-*N*-acetyl-D-hexosaminidase from *Streptococcus gordonii* [12]. Our group reported that a substrate analog, TMG-$(GlcNAc)_2$ with a *N*,*N*,*N*-trimethyl group substitution of the acetyl group of the GlcNAc at the non-reducing end of $(GlcNAc)_3$, has a K_i value of 0.077 μM against an insect β-*N*-acetyl-D-hexosaminidase OfHex1 [13]. Hatanaka et al. reported TMG-$(GlcNAc)_2$ exhibited an inhibitory activity against a bacterial β-*N*-acetyl-D-hexosaminidase from *Streptomyces coelicolor* [14] with a K_i value of 0.34 μM. PUGNAc, gluco-nagstain and NHAc-DNJ are analogs of GlcNAc where *O*-5 is replaced by a nitrogen atom in the pyranose ring and exhibit inhibitory activities against HsHex B with K_i values of 0.036, 0.01 and 0.003 μM, respectively [7,15,16]. An even weaker inhibitory activity (K_i values of 7.0 μM) of NHAc-DNJ (DNJNAc in the text) has been reported when testing against human placenta that contained both HsHexA and HsHexB [17]. The GlcNAc-type iminocyclitiol containing iminosugar and two

* Corresponding author. Tel./fax: +86 411 84707245.
** Corresponding author. Tel./fax: +86 21 64252603.
E-mail addresses: xhqian@ecust.edu.cn (X. Qian), qingyang@dlut.edu.cn (Q. Yang).

0300-9084/$ – see front matter © 2013 Elsevier Masson SAS. All rights reserved.
http://dx.doi.org/10.1016/j.biochi.2013.10.008

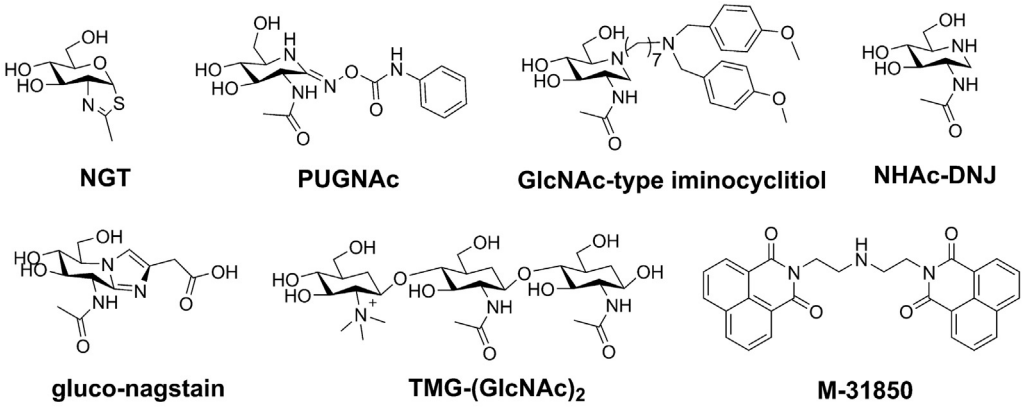

Fig. 1. Reported GH20 β-*N*-acetyl-D-hexosaminidases inhibitors.

methoxyphenyl groups with an alkylamine chain has the lowest K_i value of 0.69 nM against HsHexB [18]. Comparing with non-carbohydrate-based structure, it is more challenging to drive these leads into large-scale application because of poor physico-chemical properties and complex synthetic chemistry, in particular the difficulties in further optimization by medicinal chemistry [19,20].

Non-carbohydrate-based naphthalimides are important aromatic heterocycles chemicals with simple synthetic chemistry and immense pharmacological significances as they serve as core scaffolds for many drugs [21,22]. Naphthalimide derivatives have been reported to be efficient inhibitors of HsHex. For example, the dinaphthalimides compound **M-31850**, found by high-throughput screening [23], exhibits an IC_{50} value of 0.6 μM against HsHex. The structure–activity relationship analysis of both the compound **M-31850** and its derivatives with different linkers, suggests that one naphthalimide group might directly bind the active site, while the second naphthalimide might bind a hydrophobic patch that is away from the active pocket to provide additional weak interactions. Furthermore, an appropriately-sized *N*-alkylamine linker is presumed but not identified to be necessary to span the two binding sites. And the amine group in the linker probably donates hydrogen atom to form hydrogen bonds with active site residues. This presumption is partially proved by our recent work on the development of naphthalimides against HsHex [24].

The fact that residues forming the active pocket of HsHex are conserved in OfHex2 inspired us to deduce that the naphthalimide derivatives might be exploited as inhibitors against OfHex2. Binding affinity analysis of **M-31850** against OfHex2 confirmed **M-31850** was a competitive inhibitor of OfHex2. Ligand efficiency (LE) value, combining the binding free energy to the number of heavy atoms, is a very helpful metric guiding the optimization of hits [25]. The low LE value of **M-31850** indicated there was space to increase its efficiency. Molecular docking study suggested this low efficiency of **M-31850** was caused by the oversize of the naphthalimide group binding to the small hydrophobic cavity outside of the pocket (named out-pocket site). Thus, the improvement of the binding efficiency in the out-pocket site could be a way to increase inhibitors binding affinity.

To improve the ligand efficiency, a series of novel derivatives were synthesized by replacing one of the naphthalimide in **M-31850** with small aromatic rings to afford new unsymmetrical dyads. Optimization on the size of aromatic rings and the length of linker was performed to improve the binding affinity of moieties that bind outside of the active pocket.

The enzymatic testing and efficiency analysis suggested these new unsymmetrical dyads were competitive inhibitors of OfHex2 and had higher ligand efficiency and better inhibitory activity when compared to **M-31850**. The structure–activity relationship analysis as well as molecular docking studies provided a binding model between these inhibitors and OfHex2. And tryptophan fluorescent assay indicated that the competitive inhibition benefited from the stacking interactions between naphthalimides and tryptophan residues in the active pocket.

2. Experimental section

2.1. Chemistry

2.1.1. General

All chemicals or reagents (except specially noted) were purchased from standard commercial supplies and treated with standard methods before use. Solvents were dried in a routine way and redistilled. All melting points (m.p.) were obtained with Büchi Melting Point B540 and are uncorrected. ^1H and ^{13}C NMR spectra were recorded on a Brucker AM-400 (400 MHz) spectrometer with $CDCl_3$ or DMSO-d_6 as the solvent and TMS as the internal standard. Chemical shifts are reported in δ (parts per million) values. Coupling constants ^nJ are reported in Hz. High-resolution mass spectra (HRMS) were recorded under electron impact (70 eV) condition using a MicroMass GCT CA 055 instrument. Analytical thin-layer chromatography (TLC) was carried out on precoated plates (silica gel 60 F254), and spots were visualized with ultraviolet (UV) light. The mixtures were separated by gravity chromatography.

2.1.2. Experimental details and characterization of compounds

Compounds **1** and **2** were obtained with the similar synthetic procedure reported by Ott [26].

*2.1.2.1. 2,2′-(Azanediylbis(ethane-2,1-diyl))bis(1H-benzo[de]isoquinoline-1,3(2H)-dione) (**1**).* White solid. mp: 240–241 °C. ^1H NMR (400 MHz, $CDCl_3$): $\delta = 8.38$ (d, $J = 7.2$ Hz, 4H), 8.15 (d, $J = 8.0$ Hz, 4H), 7.64 (dd, $J = 8.0$, 7.2 Hz, 4H), 4.32 (t, $J = 6.4$ Hz, 4H), 3.10 (t, $J = 6.4$ Hz, 4H), 1.53 ppm (s, 1H); ^{13}C NMR (100 MHz, $CDCl_3$): $\delta = 164.4$, 133.7, 131.5, 131.1, 128.2, 126.8, 122.7, 47.4, 39.8 ppm; HRMS-ESI (m/z): calcd for $C_{28}H_{22}N_3O_4$ $[M + H]^+$, 464.1610; found, 464.1604.

*2.1.2.2. 2,2′-((Ethane-1,2-diylbis(azanediyl))bis(ethane-2,1-diyl))bis(1H-benzo[de]isoquinoline-1,3(2H)-dione) (**2**).* White solid. mp: decomposition (192 °C). ^1H NMR (400 MHz, $CDCl_3$): $\delta = 8.54$ (d, $J = 7.2$ Hz, 4H), 8.15 (d, $J = 8.0$ Hz, 4H), 7.70 (dd, $J = 8.0$, 7.2 Hz, 4H),

4.28 (t, J = 6.4 Hz, 4H), 2.98 (t, J = 6.4 Hz, 4H), 2.82 (s, 4H), 1.91 ppm (s, 2H); ^{13}C NMR (100 MHz, $CDCl_3$): δ = 164.3, 133.8, 131.5, 131.2, 128.1, 126.8, 122.6, 48.9, 47.5, 39.9 ppm; HRMS-ESI (m/z): calcd for $C_{30}H_{27}N_4O_4$ $[M + H]^+$, 507.2032; found, 507.2036.

2.1.3. The synthetic route of compound ***6b***

*2.1.3.1. 5′-Methoxy-5,5-dimethylspiro[[1,3]dioxane-2,3′-indolin]-2′-one (**3b**).* 5-Methoxyindoline-2,3-dione (317 mg, 1.79 mmol), neopentyl glycol (186 mg, 1.79 mmol) and *p*-toluenesulfonic acid (31 mg, 0.18 mmol) was mixed in 15 mL toluene and stirred at reflux for 8 h. After being cooled to room temperature, the mixture was filtrated. The filtrate was concentrated in vacuo to give a residue, which was purified by silica gel column chromatography to give the desired product (300 mg, 1.14 mmol) as orange solid. Yield: 64%. ^{1}H NMR (400 MHz, $CDCl_3$): δ = 8.20 (s, 1H), 7.06 (d, J = 2.4 Hz, 1H), 6.82 (dd, J = 2.4, 8.0 Hz, 1H), 6.70 (d, J = 8.0 Hz, 1H), 4.73 (d, J = 10.8 Hz, 2H), 3.80 (s, 3H), 3.55 (d, J = 10.8 Hz, 2H), 1.43 (s, 3H), 0.91 ppm (s, 3H); ^{13}C NMR (100 MHz, $CDCl_3$): δ = 173.7, 156.3, 133.5, 128.4, 116.4, 110.9, 110.4, 93.7, 71.3, 55.9, 30.3, 23.0, 22.1 ppm.

*2.1.3.2. 1′-(2-Bromoethyl)-5′-methoxy-5,5-dimethylspiro[[1,3]dioxane-2,3′-indolin]-2′-one (**4b**).* 60% Sodium hydride (182 mg, 7.60 mmol) was added portionwise to a mixture of **3b** (1.0 g, 3.80 mmol) dissolved in 20 mL DMF. After the reaction medium was stirred at 40 °C for 1 h, 1,2-dibromoethane (1.64 mL, 18.99 mmol) was then added. The reaction medium was stirred at 40 °C until the completion of reaction was detected by TLC. After extraction with ethyl acetate, the organic layer was washed with water. The organic fraction was dried over Na_2SO_4, and concentrated in vacuo to give a residue, which was purified by silica gel column chromatography to give desired product (1.3 g, 3.51 mmol, 92%) as yellowish solid. ^{1}H NMR (400 MHz, $CDCl_3$): δ = 7.07 (d, J = 2.8 Hz, 1H), 6.87 (dd, J = 2.8, 8.4 Hz, 1H), 6.74 (d, J = 8.4 Hz, 1H), 4.72 (d, J = 10.8 Hz, 2H), 3.99 (t, J = 7.2 Hz, 2H), 3.81 (s, 3H), 3.55–3.48 (m, 4H), 1.42 (s, 3H), 0.89 ppm (s, 3H); ^{13}C NMR (100 MHz, $CDCl_3$): δ = 171.1, 156.6, 135.0, 127.9, 116.0, 110.8, 109.1, 93.3, 71.4, 55.9, 41.2, 30.3, 27.0, 23.0, 22.1 ppm.

*2.1.3.3. 2-(2-((2-(5′-Methoxy-5,5-dimethyl-2′-oxospiro[[1,3]dioxane-2,3′-indolin]-1′-yl)ethyl)amino)ethyl)-1H-benzo[de]isoquinoline-1,3(2H)-dione (**5b**).* Potassium carbonate (859 mg, 6.21 mmol) was added to a solution of 7 (1.12 g, 4.66 mmol) and **4b** (1.15 g, 3.11 mmol) in 30 mL acetonitrile. The mixture was stirred at reflux until the completion of reaction was detected by TLC and then the undissolved substance was removed by filtration. The filtrate was concentrated in vacuo to give a residue, which was purified by silica gel column chromatography to give desired product (900 mg, 1.70 mmol, 55%) as yellowish solid. ^{1}H NMR (400 MHz, $CDCl_3$): δ = 8.55 (d, J = 7.2 Hz, 2H), 8.18 (d, J = 7.6 Hz, 2H), 7.72 (dd, J = 7.2, 7.6 Hz, 2H), 7.00 (d, J = 1.6 Hz, 1H), 6.82-6.72 (m, 2H), 4.67 (d, J = 11.2 Hz, 2H), 4.32 (d, J = 6.4 Hz, 2H), 3.77 (s, 3H), 3.70 (t, J = 6.4 Hz, 2H), 3.43 (d, J = 11.2 Hz, 2H), 3.06 (d, J = 6.4 Hz, 2H), 2.98 (d, J = 6.4 Hz, 2H), 1.95 (s, 1H), 1.38 (s, 3H), 0.83 ppm (s, 3H); ^{13}C NMR (100 MHz, $CDCl_3$): δ = 171.4, 164.3, 156.3, 135.8, 133.9, 131.5, 131.2, 128.1, 127.9, 126.9, 122.6, 115.9, 110.5, 109.5, 93.4, 71.2, 56.9, 47.3, 46.5, 39.7, 39.6, 30.2, 23.0, 22.1 ppm.

*2.1.3.4. 2-(2-((2-(5-Methoxy-2,3-dioxoindolin-1-yl)ethyl)amino)ethyl)-1H-benzo[de]isoquinoline-1,3(2H)-dione (**6b**).* **5b** (400 mg, 0.76 mmol) was stirred at room temperature in a mixture of HCl-AcOH (3:1 = v/v, 20 mL) for 30 min. The resulting mixture was poured into saturated sodium bicarbonate solution and extracted with dichloromethane. The organic layer was washed with water, dried over Na_2SO_4, and concentrated in vacuo to give a residue, which was purified by silica gel column chromatography to give **6b** (300 mg, 0.68 mmol, 90%) as red solid. mp 169–170 °C; ^{1}H NMR (400 MHz, $CDCl_3$): δ = 8.52 (d, J = 7.2 Hz, 2H), 8.20 (d, J = 7.6 Hz, 2H), 7.74 (dd, J = 7.2, 7.6 Hz, 2H), 7.04–6.97 (m, 2H), 6.95 (d, J = 8.0 Hz, 1H), 4.31 (t, J = 6.4 Hz, 2H), 3.79 (t, J = 6.4 Hz, 2H), 3.76 (s, 3H), 3.14–3.00 (m, 4H), 2.31 ppm (s, 1H); ^{13}C NMR (100 MHz, $CDCl_3$): δ = 183.7, 164.4, 158.6, 156.2, 145.1, 134.0, 131.5, 131.3, 128.1, 126.9, 124.6, 122.4, 117.9, 111.6, 109.3, 55.9, 47.4, 46.5, 40.3, 39.4 ppm; HRMS-ESI (m/z): calcd for $C_{25}H_{22}N_3O_5$ $[M + H]^+$, 444.1559; found,444.1560.

The compounds **6a** and **6c**–**d** were synthesized following the similar procedures as **6b**.

*2.1.3.5. 2-(2-((2-(2,3-Dioxoindolin-1-yl)ethyl)amino)ethyl)-1H-benzo[de]isoquinoline-1,3(2H)-dione (**6a**).* Yiled: 72%. Orange solid. mp 82–84 °C; ^{1}H NMR (400 MHz, $CDCl_3$): δ = 8.56 (d, J = 7.6 Hz, 2H), 8.23 (d, J = 8.0 Hz, 2H), 7.77 (dd, J = 7.6, 8.0 Hz, 2H), 7.51 (d, J = 7.6 Hz, 1H), 7.46 (dd, J = 7.2, 7.6 Hz, 1H), 7.05–6.95 (m, 2H), 4.32 (t, J = 6.4 Hz, 2H), 3.82 (t, J = 6.4 Hz, 2H), 3.00–3.10 ppm (m, 4H); ^{13}C NMR (100 MHz, $CDCl_3$): δ = 183.4, 164.5, 158.5, 151.2, 138.2, 134.0, 131.6, 131.3, 128.2, 127.0, 125.1, 123.4, 122.5, 117.6, 110.5, 47.5, 46.5, 40.5, 39.6 ppm; HRMS-ESI (m/z): calcd for $C_{24}H_{20}N_3O_4$ $[M + H]^+$, 414.1454; found, 414.1454.

*2.1.3.6. 6-(Dimethylamino)-2-(2-((2-(2,3-dioxoindolin-1-yl)ethyl)amino)ethyl)-1H-benzo[de]isoquinoline-1,3(2H)-dione (**6c**).* Yield: 91%. Red solid. ^{1}H NMR (400 MHz, $CDCl_3$): δ = 8.53 (d, J = 7.2 Hz, 1H), 8.40–8.50 (m, 2H), 7.68 (dd, J = 7.6, 8.0 Hz, 1H), 7.54 (d, J = 7.6 Hz, 1H), 7.49 (dd, J = 7.6, 8.0 Hz, 1H), 7.13 (d, J = 8.0 Hz, 1H), 7.00–7.40 (m, 2H), 4.31 (t, J = 6.0 Hz, 2H), 3.85 (t, J = 6.0 Hz, 2H), 3.14 (s, 6H), 3.07 ppm (t, J = 6.0 Hz, 4H); ^{13}C NMR (100 MHz, $CDCl_3$): δ = Gp-156-125; HRMS-ESI (m/z): calcd for $C_{26}H_{25}N_4O_4$ $[M + H]^+$, 457.1876; found, 457.1877.

*2.1.3.7. 2-(2-((2-(2,3-Dioxoindolin-1-yl)ethyl)amino)ethyl)-6-methoxy-1H-benzo[de]isoquinoline-1,3(2H)-dione (**6d**).* Yield: 56%. Yellow solid. ^{1}H NMR (400 MHz, $CDCl_3$): δ = 8.61–8.51 (m, 2H), 8.50 (d, J = 8.4 Hz, 1H), 7.70 (dd, J = 7.6, 8.0 Hz, 1H), 7.50 (d, J = 7.2 Hz, 1H), 7.45 (dd, J = 7.6, 8.0 Hz, 1H), 7.04 (d, J = 8.0 Hz, 1H), 7.02–6.96 (m, 2H), 4.28 (t, J = 6.0 Hz, 2H), 4.14 (s, 3H), 3.80 (t, J = 6.0 Hz, 2H), 3.10–2.97 ppm (m, 4H); ^{13}C NMR (100 MHz, $CDCl_3$): δ = 183.4, 164.8, 164.2, 161.0, 158.5, 151.3, 138.2, 133.6, 131.6, 129.4, 128.8, 126.0, 125.1, 123.5, 123.4, 122.2, 117.6, 114.9, 110.5, 105.2, 56.2, 47.6, 46.5, 40.5, 39.5 ppm; HRMS-ESI (m/z): calcd for $C_{25}H_{22}N_3O_5$ $[M + H]^+$, 444.1559; found, 444.1564.

*2.1.3.8. 2-(2-Aminoethyl)-1H-benzo[de]isoquinoline-1,3(2H)-dione (**7**).* 1,2-diaminoethane (0.24 mL, 3.63 mmol) was added to a suspension of 1,8-naphthalic anhydride (240 mg, 1.21 mmol) in 10 mL ethanol. The mixture was refluxed for about 4 h until the completion was detected by TLC. Then the hot reaction mixture filtered, the filtrate was cooled to room temperature and filtered again to get the crude product. The crude product was purified by recrystallization in ethanol to get 7 (150 mg, 52%) as slightly yellow solid. R_f = 0.38 ($CHCl_3$/MeOH, 10:1); mp: 141–142 °C; ^{1}H NMR (400 MHz, DMSO-d_6): δ = 8.34 (d, J = 7.6 Hz, 2H), 8.31 (d, J = 8.0 Hz, 2H), 7.75 (dd, J = 8.0, 7.6 Hz, 2H), 4.01 (t, J = 6.8 Hz, 2H), 2.79 (t, J = 6.8 Hz, 2H), 2.62 ppm (br, 2H); ^{13}C NMR (100 MHz, DMSO-d_6): δ = 163.9, 134.4, 131.5, 130.9, 127.7, 127.4, 122.4, 43.2, 40.2 ppm; HRMS-ESI (m/z): calcd for $C_{14}H_{13}N_2O_2$ $[M + H]^+$, 241.0977; found, 241.0978.

*2.1.3.9. 2-(2-((2-Aminoethyl)amino)ethyl)-1H-benzo[de]isoquinoline-1,3(2H)-dione (**8**).* Compounds 8 were synthesized following the same procedures as 7. White solid. mp: 54–56 °C. ^{1}H NMR (400 MHz, $CDCl_3$): δ = 8.54 (d, J = 6.8 Hz, 2H), 8.17 (d, J = 8.0 Hz, 4H), 7.71 (t, J = 7.6 Hz, 2H), 4.32 (t, J = 6.0 Hz, 2H), 3.01 (t, J = 6.4 Hz,

2H), 2.77 ppm (s, 4H); ^{13}C NMR (100 MHz, $CDCl_3$): δ = 164.0, 133.6, 131.2, 130.9, 127.8, 126.6, 122.2, 51.8, 47.2, 41.4, 39.7 ppm; EI MS (*m*/*e*): 284.6 (M + 1, 100). HRMS-ESI (*m*/*z*): calcd for $C_{16}H_{18}N_3O_2$ $[M + H]^+$, 284.1399; found, 284.1402.

*2.1.3.10. 2-(2-(Benzylamino)ethyl)-1H-benzo[de]isoquinoline-1,3(2H)-dione (**13**).* Potassium carbonate (120 mg, 0.87 mmol) was added to a solution of 7 (316 mg, 1.32 mmol) and (bromomethyl) benzene (74 mg, 0.43 mmol) in 10 mL acetonitrile. The mixture was stirred at reflux until the completion of reaction was detected by TLC and then the undissolved substance was removed by filtration. The filtrate was concentrated in vacuo to give a residue, which was purified by silica gel column chromatography using CH_2Cl_2/CH_3OH (30:1) to give 13 (98 mg, 0.30 mmol, 68%) as white solid. mp: 110–111 °C. ^{1}H NMR (400 MHz, $CDCl_3$): δ = 8.60 (d, *J* = 7.6 Hz, 2H), 8.22 (d, *J* = 8.0 Hz, 2H), 7.76 (dd, *J* = 8.0, 7.6 Hz, 2H), 7.32 (d, *J* = 7.6 Hz, 2H), 7.26 (dd, *J* = 7.6, 7.2 Hz, 2H), 7.19 (t, *J* = 7.2 Hz, 1H), 4.39 (t, *J* = 6.4 Hz, 2H), 3.90 (s, 2H), 3.06 (t, *J* = 6.4 Hz, 2H), 2.45 ppm (br, 1H); ^{13}C NMR (100 MHz, $CDCl_3$): δ = 164.5, 139.4, 134.0, 131.6, 131.3, 128.4, 128.3, 128.2, 127.0, 126.9, 122.6, 53.3, 46.9, 39.7 ppm; HRMS-ESI (*m*/*z*): calcd for $C_{21}H_{19}N_2O_2$ $[M + H]^+$, 331.1447; found, 331.1442.

*2.1.3.11. 2-(2-((Pyridin-2-ylmethyl)amino)ethyl)-1H-benzo[de]isoquinoline-1,3(2H)-dione (**14**).* A solution of picolinaldehyde (200 mg, 1.87 mmol) in 30 mL methanol was added to a solution of 7 (408 mg, 1.70 mmol) in 30 mL methanol. The mixture was stirred at room temperature for 3 h. The white solid in the reaction mixture was filtered and dried over infrared oven to afford the intermediate (530 mg, 1.61 mmol, 95%) as white solid. Sodium triacetoxyborohydride (219 mg, 1.03 mmol) was added to a solution of the intermediate (283 mg, 0.86 mmol) and AcOH (0.05 mL, 2.08 mmol) in 15 mL 1,2-dichloroethane. The mixture was stirred at room temperature overnight and then treated with water (50 mL) and extracted with dichloromethane (50 mL*3). The organic layer was dried over Na_2SO_4, and concentrated in vacuo to give a residue, which was purified by silica gel column chromatography using CH_2Cl_2/CH_3OH (20:1) to give 14 (222 mg, 0.67 mmol, 78%) as white solid. mp: 128–129 °C. ^{1}H NMR (400 MHz, $CDCl_3$): δ = 8.59 (t, *J* = 7.6 Hz, 2H), 8.48 (d, *J* = 4.4 Hz, 1H), 8.21 (d, *J* = 8.4 Hz, 2H), 7.75 (dd, *J* = 8.4, 7.6 Hz, 2H), 7.58 (t, *J* = 7.6 Hz, 1H), 7.30 (d, *J* = 8.0 Hz, 1H), 7.10 (dd, *J* = 8.0, 6.0 Hz, 1H), 4.40 (t, *J* = 6.4 Hz, 2H), 4.00 (s, 2H), 3.07 (t, *J* = 6.4 Hz, 2H), 2.25 ppm (s, 1H); ^{13}C NMR (100 MHz, $CDCl_3$): δ = 164.2, 159.4, 149.2, 136.4, 133.8, 131.4, 131.1, 128.0, 126.8, 122.5, 122.3, 121.9, 54.5, 47.2, 39.8 ppm; HRMS-ESI (*m*/*z*): calcd for $C_{20}H_{18}N_3O_2$ $[M + H]^+$, 332.1399; found, 332.1401.

The compounds **15** and **16** were synthesized following the same procedures as **14**.

*2.1.3.12. 2-(2-((4-(Trifluoromethyl)benzyl)amino)ethyl)-1H-benzo[de]isoquinoline-1,3(2H)-dione (**15**).* Yield: 80%. White solid. mp: 135–138 °C. ^{1}H NMR (400 MHz, $CDCl_3$): δ = 8.56 (d, *J* = 6.8 Hz, 2H), 8.19 (d, *J* = 8.0 Hz, 2H), 7.23 (dd, *J* = 8.0, 6.8 Hz, 2H), 7.47 (d, *J* = 8.0 Hz, 2H), 7.39 (d, *J* = 8.0 Hz, 2H), 4.36 (t, *J* = 6.4 Hz, 2H), 3.90 (s, 2H), 3.01 (t, *J* = 6.4 Hz, 2H), 1.56 ppm (s, 1H); ^{13}C NMR (100 MHz, $CDCl_3$): δ = 164.4, 144.6, 134.0, 131.6, 131.3, 129.0 (q, *J* = 32.3 Hz), 128.3, 128.2, 127.0, 125.2 (q, *J* = 3.7 Hz), 124.3 (q, *J* = 271.9 Hz), 122.6, 52.9, 47.1, 39.9 ppm; HRMS-ESI (*m*/*z*): calcd for $C_{22}H_{18}N_2O_2F_3$ $[M + H]^+$, 399.1320; found, 399.1324.

*2.1.3.13. 2-(2-((4-(Dimethylamino)benzyl)amino)ethyl)-1H-benzo[de]isoquinoline-1,3(2H)-dione (**16**).* Orange solid. Yield: 70‰ ^{1}H NMR (400 MHz, DMSO-d_6): δ = 8.59 (s, 1H), 8.52 (d, *J* = 7.6 Hz, 2H), 8.50 (d, *J* = 7.6 Hz, 2H), 7.90 (t, *J* = 7.6 Hz, 2H), 7.27 (d, *J* = 7.6 Hz, 2H), 6.72 (d, *J* = 7.6 Hz, 2H), 4.39 (t, *J* = 6.4 Hz, 2H), 4.08 (s, 2H), 3.29 (t, *J* = 6.4 Hz, 2H), 2.89 ppm (s, 6H); ^{13}C NMR (100 MHz, DMSO-d_6): δ = 164.0, 150.7, 134.4, 131.2, 130.9, 130.7, 127.5, 127.2, 122.2, 118.1, 111.9, 54.8, 50.2, 44.8, 36.4 ppm; HRMS-ESI (*m*/*z*): calcd for $C_{23}H_{24}N_3O_2$ $[M + H]^+$, 374.1869; found, 374.1873.

*2.1.3.14. 2-(2-(Dibenzylamino)ethyl)-1H-benzo[de]isoquinoline-1,3(2H)-dione (**17**).* Potassium carbonate (155 mg, 1.12 mmol) was added to a solution of 7 (162 mg, 0.68 mmol) and (bromomethyl) benzene (231 mg, 1.35 mmol) in 10 mL acetonitrile. The mixture was stirred at reflux until the completion of reaction was detected by TLC and then the undissolved substance was removed by filtration. The filtrate was concentrated in vacuo to give a residue, which was purified by silica gel column chromatography using CH_2Cl_2/CH_3OH (40:1) to give 17 (252 mg, 0.61 mmol, 89%) as white solid. mp: 119–120 °C. ^{1}H NMR (400 MHz, $CDCl_3$): δ = 8.52 (d, *J* = 7.6 Hz, 2H), 8.23 (d, *J* = 8.0 Hz, 2H), 7.77 (dd, *J* = 8.0, 7.6 Hz, 2H), 7.24–7.17 (m, 4H), 7.05–6.95 (m, 6H), 4.38 (t, *J* = 6.0 Hz, 2H), 3.64 (s, 4H), 2.82 ppm (t, *J* = 6.0 Hz, 2H); ^{13}C NMR (100 MHz, $CDCl_3$): δ = 163.9, 139.6, 133.7, 131.5, 131.0, 128.9, 128.2, 128.0, 126.9, 126.6, 122.9, 58.3, 51.2, 37.9 ppm; HRMS-ESI (*m*/*z*): calcd for $C_{28}H_{25}N_2O_2$ $[M + H]^+$, 421.1916; found, 421.1911.

The compounds **18**–**21** and **9**–**10** were synthesized following the similar procedures as **13**.

*2.1.3.15. 2-(2-(Phenethylamino)ethyl)-1H-benzo[de]isoquinoline-1,3(2H)-dione (**18**).* Yield: 71%. White solid. mp: 94–95 °C. ^{1}H NMR (400 MHz, $CDCl_3$): δ = 8.66 (d, *J* = 7.6 Hz, 2H), 8.30 (d, *J* = 8.0 Hz, 2H), 7.84 (dd, *J* = 8.0, 7.6 Hz, 2H), 7.34–7.27 (m, 4H), 7.24 (t, *J* = 6.4 Hz, 1H), 4.49 (t, *J* = 6.4 Hz, 2H), 3.22 (t, *J* = 6.4 Hz, 2H), 3.16 (t, *J* = 7.2 Hz, 2H), 3.00 ppm (t, *J* = 7.2 Hz, 2H); ^{13}C NMR (100 MHz, $CDCl_3$): δ = 164.5, 139.0, 134.1, 131.6, 131.4, 128.8, 128.5, 128.2, 126.9, 126.2, 122.5, 50.4, 47.3, 39.1, 35.3 ppm; HRMS-ESI (*m*/*z*): calcd for $C_{22}H_{21}N_2O_2$ $[M + H]^+$, 345.1603; found, 345.1601.

*2.1.3.16. 2-(2-((3-Phenylpropyl)amino)ethyl)-1H-benzo[de]isoquinoline-1,3(2H)-dione (**19**).* Yield: 75%. White solid. mp: 47–48 °C. ^{1}H NMR (400 MHz, $CDCl_3$): δ = 8.63 (d, *J* = 7.6 Hz, 2H), 8.25 (d, *J* = 8.4 Hz, 2H), 7.78 (dd, *J* = 8.4, 7.6 Hz, 2H), 7.25 (d, *J* = 7.2 Hz, 2H), 7.21–7.13 (m, 3H), 4.40 (t, *J* = 6.4 Hz, 2H), 3.07 (t, *J* = 6.4 Hz, 2H), 2.79 (t, *J* = 7.2 Hz, 2H), 2.67 (t, *J* = 7.6 Hz, 2H), 2.20 (br, 1H), 1.88 ppm (dt, *J* = 7.6, 7.2 Hz, 2H); ^{13}C NMR (100 MHz, $CDCl_3$): δ = 164.2, 142.1, 133.8, 131.4, 131.2, 128.4, 128.3, 128.0, 126.8, 125.7, 122.5, 49.1, 47.7, 40.0, 33.5, 31.6 ppm; HRMS-ESI (*m*/*z*): calcd for $C_{23}H_{23}N_2O_2$ $[M + H]^+$, 359.1760; found, 359.1758.

*2.1.3.17. 2-(2-((2-Phenoxyethyl)amino)ethyl)-1H-benzo[de]isoquinoline-1,3(2H)-dione (**20**).* Yield: 71%. White solid. mp: 112–114 °C. ^{1}H NMR (400 MHz, $CDCl_3$): δ = 8.59 (d, *J* = 7.6 Hz, 2H), 8.20 (d, *J* = 8.0 Hz, 2H), 7.74 (dd, *J* = 8.0, 7.6 Hz, 2H), 7.24 (t, *J* = 7.6 Hz, 2H), 6.91 (t, *J* = 7.2 Hz, 1H), 6.87 (d, *J* = 8.0 Hz, 2H), 4.37 (t, *J* = 6.8 Hz, 2H), 4.05 (t, *J* = 4.8 Hz, 2H), 3.14–3.04 (m, 4H), 1.83 ppm (s, 1H); ^{13}C NMR (100 MHz, $CDCl_3$): δ = 164.2, 158.8, 133.9, 131.5, 131.2, 129.4, 128.0, 126.8, 122.5, 120.7, 114.5, 67.2, 48.5, 47.4, 39.9 ppm; HRMS-ESI (*m*/*z*): calcd for $C_{22}H_{21}N_2O_3$ $[M + H]^+$, 361.1552; found, 361.1548.

*2.1.3.18. 2-(2-(((5-Phenyl-1,3,4-oxadiazol-2-yl)methyl)amino)ethyl)-1H-benzo[de]isoquinoline-1,3(2H)-dione (**21**).* Yield: 60%. White solid. mp: 166–168 °C. ^{1}H NMR (400 MHz, $CDCl_3$): δ = 8.51 (d, *J* = 7.2 Hz, 2H), 8.13 (d, *J* = 7.6 Hz, 2H), 7.93 (dt, *J* = 6.8, 1.6 Hz, 2H), 7.67 (dd, *J* = 7.6, 7.2 Hz, 2H), 7.47 (tt, *J* = 7.2, 2.4 Hz, 1H), 7.41 (tt, *J* = 7.2, 1.6 Hz, 2H), 4.35 (t, *J* = 6.4 Hz, 2H), 4.14 (s, 2H), 3.13 (t, *J* = 6.4 Hz, 2H), 1.97 ppm (s, 1H); ^{13}C NMR (100 MHz, $CDCl_3$): δ = 165.0, 164.8, 164.2, 133.8, 131.4, 131.3, 131.0, 128.7, 127.9, 126.7, 126.6, 123.6, 122.2, 46.9, 43.2, 39.3 ppm; HRMS-ESI (*m*/*z*): calcd for $C_{23}H_{19}N_4O_3$ $[M + H]^+$, 399.1457; found, 399.1457.

*2.1.3.19. 2-(2-((2-(1,3-Dioxoisoindolin-2-yl)ethyl)amino)ethyl)-1H-benzo[de]isoquinoline-1,3(2H)-dione (**9**).* Yield: 70%. White solid. mp 172–174 °C; ^{1}H NMR (400 MHz, $CDCl_3$): δ = 8.49 (d, J = 7.2 Hz, 2H), 8.21 (d, J = 8.0 Hz, 2H), 7.72 (dd, J = 7.2, 8.0 Hz, 2H), 7.63 (s, 4H), 4.32 (t, J = 6.0 Hz, 2H), 3.80 (t, J = 6.0 Hz, 2H), 3.07 (t, J = 6.0 Hz, 2H), 3.02 (t, J = 6.0 Hz, 2H), 1.59 ppm (s, 1H); ^{13}C NMR (100 MHz, $CDCl_3$): δ = 168.4, 164.4, 133.8, 133.6, 132.1, 126.9, 123.0, 122.7, 47.4, 47.2, 39.7, 37.6 ppm; HRMS-ESI (m/z): calcd for $C_{24}H_{19}N_3O_4$ $[M + H]^+$, 414.1454; found, 414.1456.

*2.1.3.20. 2-(2-((2-(2-Oxobenzo[cd]indol-1(2H)-yl)ethyl)amino)ethyl)-1H-benzo[de]isoquinoline-1,3(2H)-dione (**10**).* Yellow solid. mp: 147–149 °C. ^{1}H NMR (400 MHz, $CDCl_3$): δ = 8.44 (d, J = 7.2 Hz, 2H), 8.14 (d, J = 8.0 Hz, 2H), 7.92 (d, J = 8.0 Hz, 1H), 7.87 (d, J = 6.8 Hz, 1H), 7.67 (dd, J = 8.0, 7.2 Hz, 2H), 7.61 (dd, J = 7.6, 7.2 Hz, 1H), 7.42 (d, J = 8.4 Hz, 1H), 7.33 (dd, J = 8.0, 7.6 Hz, 1H), 6.94 (d, J = 6.8 Hz, 1H), 4.29 (t, J = 6.4 Hz, 2H), 3.99 (t, J = 6.4 Hz, 2H), 3.09 (t, J = 6.4 Hz, 2H), 3.05 (t, J = 6.4 Hz, 2H), 1.76 ppm (s, 1H); ^{13}C NMR (100 MHz, $CDCl_3$): δ = 168.2, 164.3, 139.6, 133.8, 131.5, 131.1, 130.7, 129.0, 128.5, 128.5, 128.1, 126.8, 126.5, 125.1, 124.1, 122.5, 120.1, 105.3, 47.9, 47.4, 40.4, 39.7 ppm; HRMS-ESI (m/z): calcd for $C_{27}H_{22}N_3O_3$ $[M + H]^+$, 436.1661; found, 436.1668.

*2.1.3.21. 2-((2-(1,3-Dioxo-1H-benzo[de]isoquinolin-2(3H)-yl)ethyl)amino)-N-(quinolin-8-yl)acetamide (**11**).*
2-Chloro-*N*-(quinol-8-yl)acetamide (107 mg, 0.49 mmol), 7 (117 mg, 0.49 mmol), *N*,*N*-diisopropylethylamine (0.86 mL, 4.9 mmol) and potassium iodide (10 mg) were added to acetonitrile (30 mL), after stirred and refluxed for 10 h under nitrogen atmosphere, the mixture was cooled to rt and concentrated in vacuo to get crude product which was purified by silica gel column chromatography to afford 11 (140 mg, 0.33 mmol, 68%) as white solid. mp: 176–178 °C. ^{1}H NMR (400 MHz, $CDCl_3$): δ = 11.1 (s,1H), 8.75 (d, J = 7.6 Hz, 1H), 8.51 (d, J = 7.2 Hz, 2H), 8.16 (d, J = 8.0 Hz, 2H), 8.01 (d, J = 8.0 Hz, 1H), 7.99 (d, J = 4.4 Hz, 1H), 7.67 (dd, J = 8.0, 7.2 Hz, 2H), 7.48 (dd, J = 8.0, 7.6 Hz, 1H), 7.42 (d, J = 8.0 Hz, 1H), 7.16 (dd, J = 8.0, 4.4 Hz, 1H), 4.47 (t, J = 6.4 Hz, 2H), 3.64 (s, 2H), 3.21 (t, J = 6.4 Hz, 2H), 1.97 ppm (s, 1H); ^{13}C NMR (100 MHz, $CDCl_3$): δ = 170.4, 164.4, 147.9, 138.7, 135.8, 134.2, 133.8, 131.5, 131.3, 128.2, 127.8, 127.1, 126.8, 122.5, 121.5, 121.1, 116.5, 53.4, 47.9, 39.7 ppm; HRMS-ESI (m/z): calcd for $C_{25}H_{21}N_4O_3$ $[M + H]^+$, 425.1614; found, 425.1617.

*2.1.3.22. N-(2-((2-(1,3-dioxo-1H-benzo[de]isoquinolin-2(3H)-yl)ethyl)amino)ethyl)-4-methoxybenzamide (**12**).* To a mixture of 4-methoxybenzoic acid (2.0 g, 13.2 mmol) in 20 mL benzene was dropwised thionyl dichloride (4.8 mL, 65.7 mmol) at 0 °C. And then the mixture was heated and refluxed for 8 h. After completion, the reaction mixture was cooled to room temperature and concentrated under vacuum to give intermediate (2.2 g, 98%) as colorless oil. To a solution of 8 (150 mg, 0.53 mmol) and pyridine (2 mL) in 10 mL dichloromethane was dropwised a solution of intermediate obtained above (60 mg, 0.35 mmol) in 10 mL dichloromethane. The mixture was stirred at room temperature and monitored by TCL. After completion, the reaction mixture was treated with water (100 mL) and then extracted with dichloromethane (3 * 50 mL). The combined organic layers were washed with brine, dried over Na_2SO_4, and concentrated in vacuo. The residue was purified by silica gel column chromatography to give 12 (100 mg, 68%) as yellow solid. ^{1}H NMR (400 MHz, $CDCl_3$): δ = 8.39 (d, J = 6.8 Hz, 2H), 8.10 (d, J = 7.2 Hz, 2H), 7.65–7.56 (m, 4H), 7.04 (s, 1H), 6.70 (d, J = 6.4 Hz, 2H), 4.26 (t, J = 6.0 Hz, 2H), 3.75 (s, 3H), 3.80 (t, J = 6.0 Hz, 2H), 3.07 (t, J = 6.0 Hz, 2H), 3.02 (t, J = 6.0 Hz, 2H), 1.59 ppm (s, 1H); ^{13}C NMR (100 MHz, $CDCl_3$): δ = 167.2, 164.4, 161.8, 133.9, 131.4, 131.2, 128.8, 127.9, 127.0, 126.8, 122.3, 113.4, 77.5, 77.4, 77.2, 76.9, 55.3, 47.9, 47.4, 39.7 ppm; HRMS-ESI (m/z): calcd for $C_{24}H_{24}N_3O_4$ $[M + H]^+$, 418.2; found, 418.2.

2.2. Inhibitory activity and ligand efficiency analysis

The insect GH20 enzyme OfHex2 was prepared as described by Liu et al. [2] the bacterial hexosaminidase from *Serratia marcescens* and another insect hexosaminidase OfHex1 was prepared as described by Liu et al. [27]. GH20 hexosaminidases from *Trichoderma viride*, *Canavalia ensiformis* and *Homo sapiens* were purchased from Sigma–Aldrich. All of the synthesized compounds were evaluated for their inhibitory activities against hexosaminidases by using the artificial substrate, *p*NP-GlcNAc. The assay components were incubated in a final volume of 60 μl at 25 °C for 30 min in the presence of Britton-Robinson buffer(OfHex2, pH 6.0; OfHex1, TvHex, and SmHex, pH 7.0; HsHex and CeHex, pH 4.5), ethanol at the final concentration of 20%, enzyme, compounds and *p*NP-GlcNAc. Then enzyme reaction was stopped by the addition of 60 μl 0.5 M Na_2CO_3 solution. The inhibition constant (K_i [μM]) was obtained by Dixon plots by changing the concentration of the compound at a constant concentration (0.2 and 0.5 mM) of the substrate. Ligand efficiency values were calculated as follows [28]: LE = $-1.35 \log(K_i)/N$, where N is the number of heavy atoms.

2.3. Molecular modeling

Homology modeling of the catalytic domain of OfHex2 (GenBank: ABO65045.1, residues 192–503), was carried out by using SWISS-MODEL Workspace [29]. The crystal structure of HsHex (PDB code: 1O7A, chain B) with amino acid sequence identity of 48.8% of the catalytic domain of OfHex2 was used as template. The quality of the homology model was evaluated by QMEAN global score and QMEAN Z-score and estimation of the local quality was performed using graphical plots of Anolea mean force potential, GROMOS empirical force field energy and QMEAN, indicated the modeled catalytic domain of OfHex2 was reliable according to *Z*-score of −0.18 and a high QMEAN global score of 0.759 [30]. The structure of modeled catalytic domain was depicted using the software PyMol.

2.4. Molecular docking

The PRODRG2 server [31,32] has been used to generate and optimize the initial structure of our compounds before docking. The molecular docking methodology, by running autodock4.2 software [33,34], consists of two steps: the protein-ligand complex was obtained firstly by rigid docking and then by flexible docking via setting the active pocket-outside-ligand binding residues flexible. Polar hydrogen atoms and Gasteiger charges were added using AutoDockTools. All maps were calculated with 0.375 Å spacing between grid points. The centre of the grid box was placed at the centre of the active pocket of Modeled OfHex2. The dimensions of the active site box were set at 52 × 50 × 58 Å. Docking calculations were carried out using the Lamarckian genetic algorithm (LGA) and all parameters were the same for each docking. A population of random individuals (population size: 150), a maximum number of 25,000,000 energy evaluations, a maximum number of generations of 27,000 was used.

2.5. Fluorescence spectroscopy

In the tryptophan fluorescence titration experiment, compound was titrated into 100ul titration buffer (0.5 M NaCl, 20 mM Na_2HPO_4, pH 6.0) containing 0.32 mg OfHex2 from 0 to 185 μM. The samples were incubated at 298 K for various durations. The tryptophan fluorescence titration was performed in the 96 well solid

black polystyrene microplate using a Varioskan Flash (Thermo Scientific Co.). The excitation wavelength was 280 nm, and the emission data were collected between 300 and 480 nm. To determine the dissociation constant, the fluorescence changes (ΔF) at 322 nm after addition of test compounds were fit with the specific binding equation: $\Delta F = \Delta F_{max} X/(K_d + X)$, where ΔF_{max} is the maximum fluorescence changes and X is the concentration of added inhibitor [35]. This nonlinear fitting method was performed with the GraphPad Prism software program (San Diego, CA).

3. Results and discussion

3.1. Mechanism of symmetrical dyads of naphthalimide *M-31850* binding to OfHex2

Inhibitory activity testing suggested **M-31850** is a competitive inhibitor against OfHex2 with a K_i value of 2.5 μM. However, the low LE value (0.21) indicated the binding between **M-31850** and OfHex2 was not efficient enough. To study the mechanism of **M-31850** interacting with OfHex2, molecular docking was performed using the homology modeled structure of OfHex2 using HsHex as template. The molecular docking study revealed that one of the naphthalimide groups of **M-31850** localized in the active pocket and the secondary amine in the linker formed a hydrogen bond with the side chain of the residue E345. And the second naphthalimide group stacked poorly in the narrow out-pocket site. As shown in Fig. 2, only part of the imide ring and one aromatic ring of naphthaline of the second naphthalimide group stacked with the imidazole group of the residue H285 at a dihedral of about 35° in the out-pocket site, while the other aromatic ring of naphthaline group was away from the out-pocket site. The inefficiency binding in the out-pocket site might be caused by the oversize of naphthalimide group or the lack of flexibility of the linker between secondary amine and the second naphthalimide group. Thus, the second naphthalimide group is better to be replaced by a smaller group and to be conjugated by an appropriately-lengthed *N*-alkylamine linker.

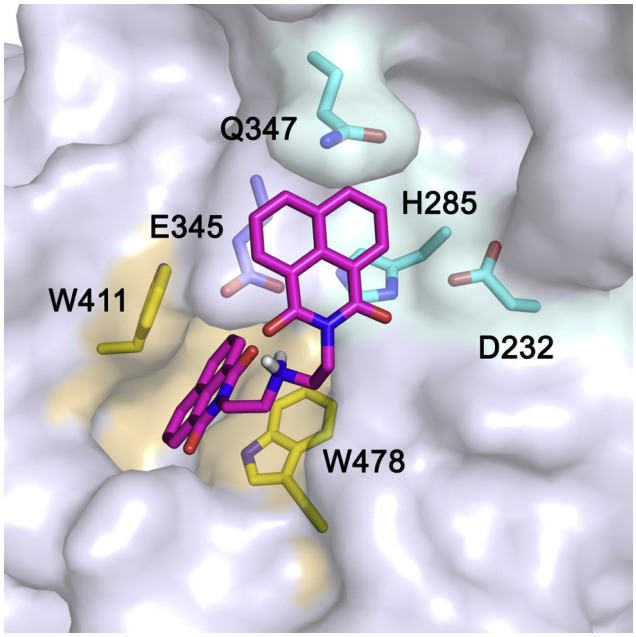

Fig. 2. Molecular docking of **M-31850** into OfHex2. The active pocket and out-pocket site were shown in light orange and pale cyan surface, respectively. The catalytic residue E345 was shown in blue stick. The compound **M-31850** was shown in magenta stick.

3.2. Synthesis of designed naphthalimides

1 and **2** were obtained by reacting a suspension of 1,8-naphthalic anhydride in ethanol with 0.5 equivalence of amines (Fig. 3).

Compound **6a**–**d** were synthesized by following steps (Fig. 4). The carbonyl-protection of isatins were generated by neopentyl glycol and tosylic acid as catalyst in toluene. After treated with sodium hydride in dry DMF, **3a** or **3b** reacted with 1,2-dibromoethane to yield bromides **4a**–**b**. The preparations of carbonyl-protected **5a**–**d** were finished by the reactions of corresponding naphthalimide derivatives with **4a** or **4b** under the condition of potassium carbonate and acetonitrile. **20a**–**d** were finally obtained by removal of the protecting group in the system of hydrochloric acid and acetic acid.

Compounds **7** and **8** were obtained by reacting a suspension of 1,8-naphthalic anhydride in ethanol with excessive amines followed by recrystallization. Compound **7** was refluxed with different bromides or chlorides and potassium carbonate in acetonitrile for 12 h to afford compounds **9**, **10**, **13** and **17-21**. Compound **7** was easily transformed into **14**–**16** by performing a Schiff condensation in methanol in the presence of equivalent of different benzaldehydes followed reducing reaction with sodium triacetoxyborohydride. Compound **11** was synthesized by conjugating **7** and 2-chloro-*N*-(quinol-8-yl)-acetamide in acetonitrile with diisopropylethylamine and potassium iodide. **8** reacted with 4-methoxybenzoyl chloride in basic condition to afford **12** (Fig. 5).

3.3. Bioevaluation of inhibitory activity

All of the synthesized compounds were evaluated for their inhibition activities against OfHex2 by using the artificial *p*NP-GlcNAc as substrate.

To improve the binding efficiency to the out-pocket site, compounds **1**–**12** containing less than three conjugate aromatic rings were synthesized (Table 1). The slightly increase in inhibitory activity of **2** suggested that the increase of linker flexibility could improve binding affinity. Compounds **6a**, and **9**–**12** possess similar structures as **1** (**M-31850**). All of them have amide and phenyl group, but are smaller than **1**. Reserving two carbonyl groups and reducing naphthyl to phenyl (**6a** and **9**) improved about 1-fold in inhibitory activity, though the ligand efficiency were little increased from 0.21 to 0.26 and 0.25, respectively. It was suggested the reduced phenyl group of **1** favored its binding. The activity loss of **10** revealed that the fragment containing three aromatic rings could not improve the affinity even if minished its size comparing with naphthalimide. The decreased inhibitory activity of **6b**, substituted with methoxy group on the 4-position of isatin group of **6a**, suggested additional substitution on this position would lead to steric hindrance. However, the change on the similar position of monocycle compound **12** remarkably improved inhibitory activity if compared with **1**. This suggested that aromatic monocycle fragment could improve the potency and the steric position of the monoaromatic ring would influence the affinity. Besides, the addition of hydrophilic group at 4-position of naphthalimide (**6c** and **6d**) significantly interfered the inhibitory activity. It indicated naphthalimide group might play an irreplaceable role for inhibitory activity.

Then, a series of aromatic monocycles compounds **13**–**21** with different linker were synthesized (Table 2). The compound **20** was identified to be the best that exhibited about 6-fold increase in inhibitory activity when compared with compound **1**. The comparison of the inhibitory activity of compounds **13** and **18**–**20**, indicated the activity improvement was linked to length of the linker between phenyl group and secondary amine. Flexible linker

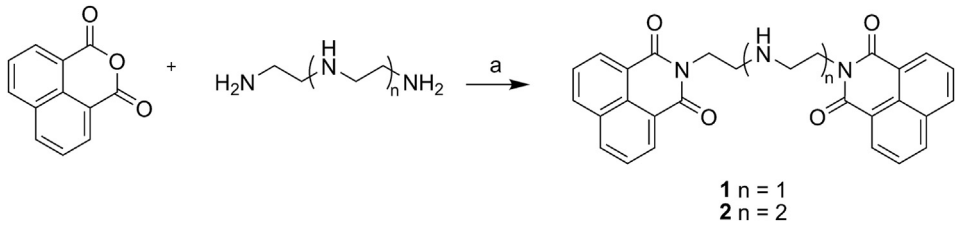

Fig. 3. Synthesis of compounds **1** and **2**. a) EtOH, reflux, 7 h.

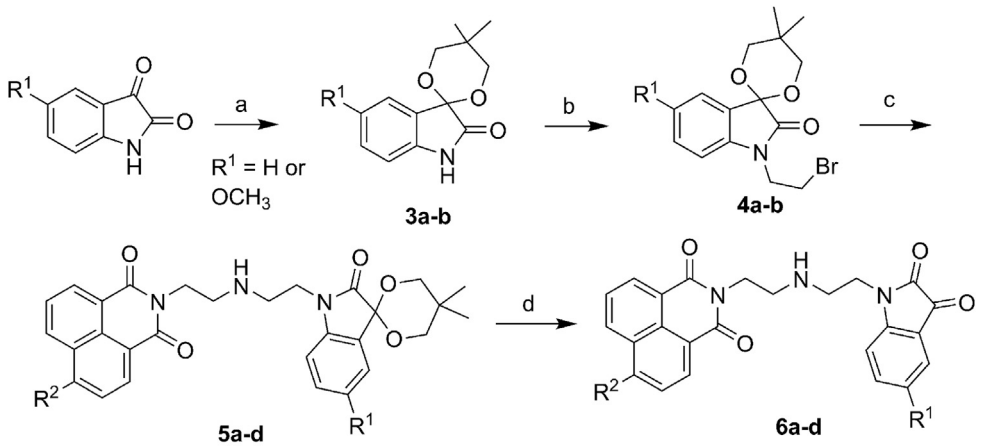

Fig. 4. Synthesis of compounds **6a**–**d**. a) NPG, TsOH, toluene, reflux, 8 h; b) NaH, $BrCH_2CH_2Br$, DMF, 40 °C, 3 h; c) K_2CO_3, MeCN, reflux, 12 h; d) AcOH, HCl, rt, 30 min.

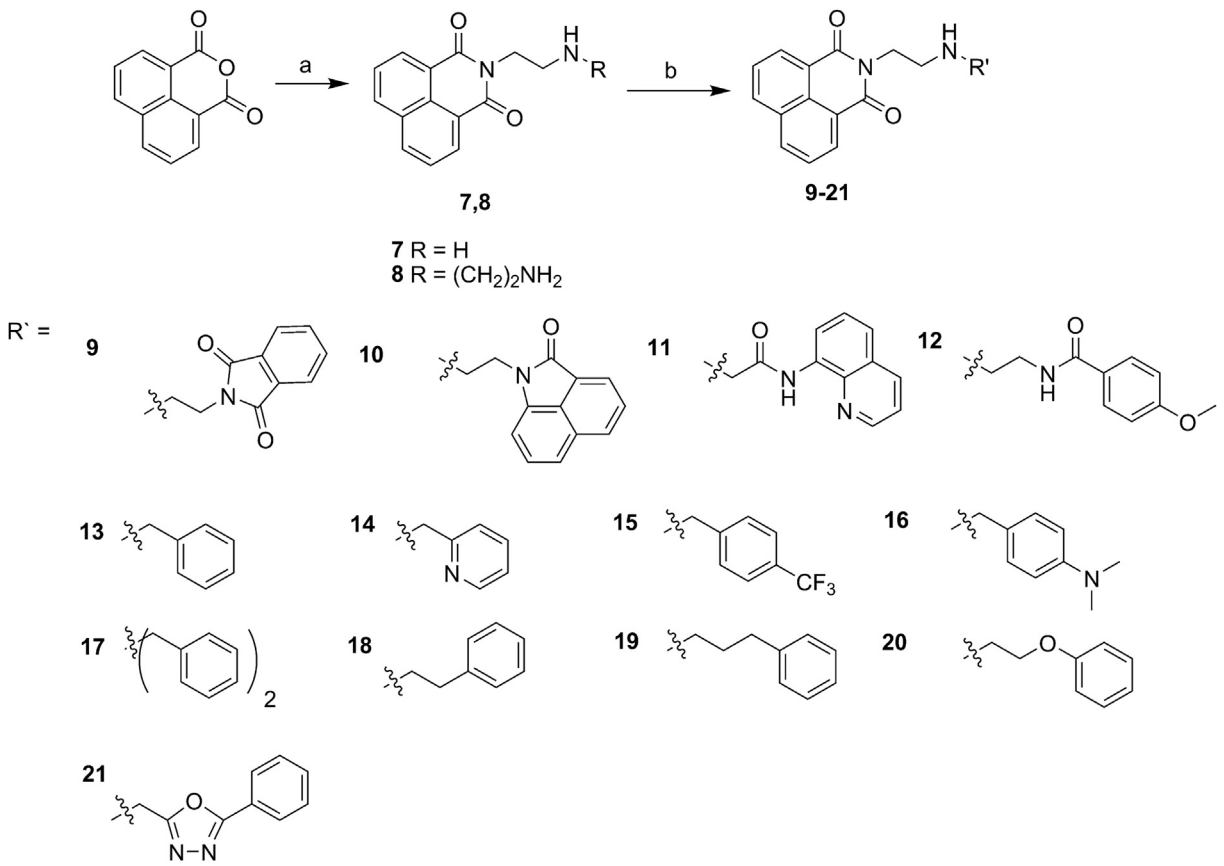

Fig. 5. Synthesis of compounds **7**–**21**. a) amines, EtOH, reflux, 4 h; b) **9**, **10**, **13** and **17**–**21**: **7**, bromides or chlorides, K_2CO_3, MeCN, reflux, 12 h; **14**–**16**: **1**, benzaldehydes, MeOH, rt, 12 h, then $NaBH(CH_3COO)_3$, AcOH, DCM, rt, 12 h; **11**: **7**, chloride, diisopropylethylamine, KI, MeCN, reflux, 10 h; **12**: **8**, acyl chloride, pyridine, rt, 12 h.

Table 1
Inhibitory activities of compounds **1**–**12** against OfHex2.

No.	R^1	R^2	K_i [μM]	LE
Parent[a]	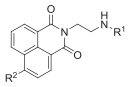			
1	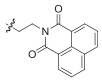	H	2.50	0.21
2	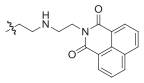	H	2.16	0.20
6a		H	1.21	0.26
6b	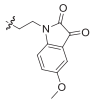	H	2.09	0.23
6c		OCH_3	N.D.[b]	–
6d		$N(CH_3)_2$	N.D.	
9		H	1.40	0.25
10		H	N.D.	–
11	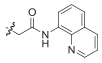	H	5.77	0.22
12	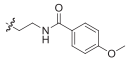	H	2.31	0.24

[a] General structure naphthalimide derivatives evaluated.
[b] Not determined because of the low activity (less than 50% inhibition at 10 μm).

Table 2
Inhibitory activities of compounds **13**–**21** against OfHex2.

No.	R	K_i [μM]	LE
Parent[a]	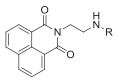		
13		1.57	0.31
14		1.74	0.31
15	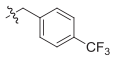	N.D.[b]	–
16	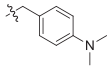	2.47	0.27
17		N.D.	–
18		1.31	0.30
19	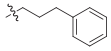	0.55	0.31
20	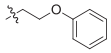	0.37	0.31
21	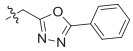	N.D.	–

[a] General structure naphthalimide derivatives evaluated.
[b] Not determined because of the low activity (less than 50% inhibition at 10 μm).

with proper length facilitated the phenyl group staking well with the hydrophobic patch outside of the active pocket. The highest inhibitory activity of **20** indicated that the oxygen in the linker might contribute an interaction. The activity loss of **21** which has an additional heterocycle on the linker also supported that the binding required a flexible linker. The approximate inhibitory activity of **13** and **14** indicated that substitution on the 2-position of the phenyl group of **13** with nitrogen atom would not influence the inhibitory activity obviously. The lower activity of **15** and **16**, the analogs of **13**, suggested that a hydrophobic group on the 4-position of the phenyl group of **13** would weaken the binding of phenyl group to the out-pocket site.

3.4. Effects of the compound **20** on β-N-acetyl-D-hexosaminidases

The inhibitory activity analysis of the compound **20**, the most potential compound in Table 2, was further performed against GH20 β-*N*-acetyl-D-hexosaminidases from bacteria (SmChb), fungi (TvHex), plant (CeHex) and human (HsHex) and the insect chitinolytic enzyme, OfHex1, as shown in Table 3. The data indicated that the compound **20** did not inhibit β-*N*-acetyl-D-hexosaminidases from either bacterium or fungi. In comparison with other β-*N*-acetyl-D-hexosaminidases, the compound **20** against OfHex2 exhibited a K_i of 0.37 μM, while against the plant CeHex with K_i of 4.88 μM, the human HsHex with K_i of 1.29 μM and the insect chitinolytic enzyme OfHex1 with K_i of 224.51 μM.

3.5. Mechanism analysis of unsymmetrical dyads of naphthalimide derivatives inhibiting OfHex2

To further understand the molecular mechanism of naphthalimide derivatives, we investigated the binding mode of the most potent compound **20**. As shown in Fig. 6, dixon plot of **20** against OfHex2 indicated **20** is a competitive inhibitor of OfHex2, because of the trendlines drawn for each concentration of substrate meeting in quadrant two. Thus, **20** could specific bind to the active pocket of OfHex2.

Molecular docking was also performed using the structure of OfHex2 constructed by the homology modeling using HsHex as template. The interactions between **20** and OfHex2 were then analyzed.

As shown in Fig. 7A, the naphthalimide group of **20** was stacking with the W478 and/or the W411 in the active pocket. The secondary

Table 3
Inhibition constants (K_i, μM) of **20** against GH20 β-*N*-acetyl-D-hexosaminidases.

SmChb	TvHex	OfHex1	OfHex2	CeHex	HsHex
N.D.[a] (5.6)[b]	N.D. (11.8)	224.51	0.37	4.88	1.29

[a] Not determined because of the low activity (less than 20% inhibition at 100 μm).
[b] Inhibition (%) at 100 μm are given in parentheses.

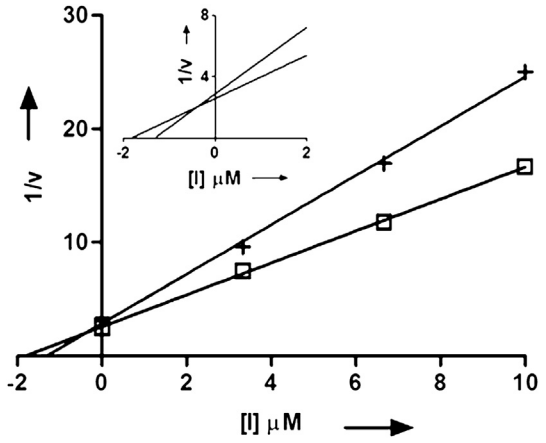

Fig. 6. Dixon plots for inhibition of OfHex2 by **20**. The trendlines represent two substrate concentrations (+, 0.2 mM; □, 0.5 mM). The insert graph is the partial enlarged view around the intersection.

amine in the linker of **20** formed hydrogen bonds with the side chain of the catalytic amino acid E345 within the distance of 2.8 Å. It was worth to note the phenyl group of **20** might stack with two different hydrophobic patch consisted of (I) the residues W411 and Y436, or (II) H285.

The stacking with hydrophobic patch (I) was observed both in rigid-body docking and flexible docking by setting the residues W411, Y436 and H439 flexible. But the stacking with the patch (II) was only observed in flexible docking. This might be due to the steric hindrance in active pocket caused by the side chain of Y436. Interestingly, Y436 (Y450 in HsHex B) and H439 (L454 in HsHex B) were located in a loop. Like in the β-*N*-acetyl-D-hexosaminidase from *Streptococcus pneumonia* (PDB code: 3RPM) [36], these two residues were close enough to form a stacking interaction. And the shift of Y436 was also observed in the comparison of the crystal complexes of HsHexB:NGT and HsHexB:PYR [37]. In comparison with OfHex2, inhibitory activities of **20** against OfHex1 and SmChb dramatically decreased. This might be due to the residue H285 was not solvent exposed in OfHex1 (H303) and SmChb (H452) [27,38]. As a result the naphthalimide group would insert more deeply in the pocket, forming a sandwiched stacking interaction with both

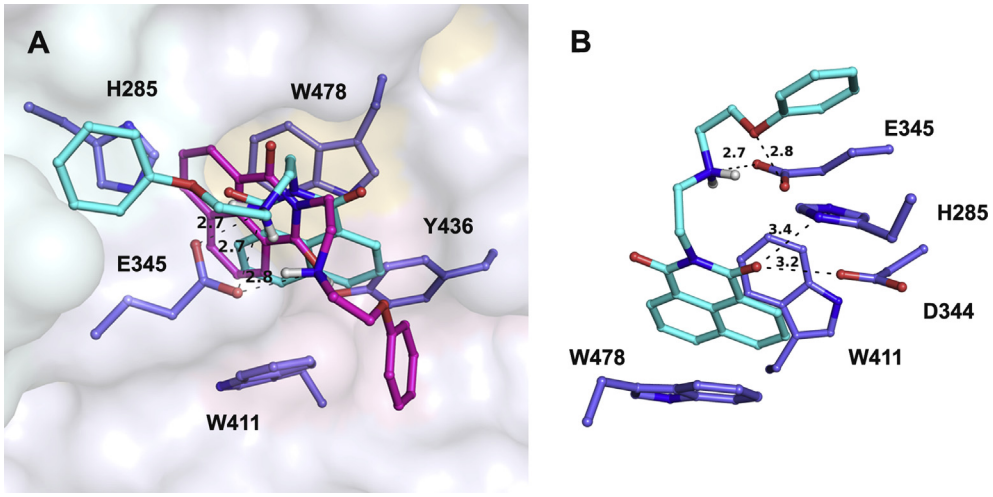

Fig. 7. Molecular docking of **20** against OfHex2. Hydrophobic patch (I) and (II) were colored pale cyan and light pink, respectively. Residues were shown in slate sticks. A) Two conformations of **20** were shown in cyan and magenta sticks. B) The interaction between **20** of conformation (I) and OfHex2.

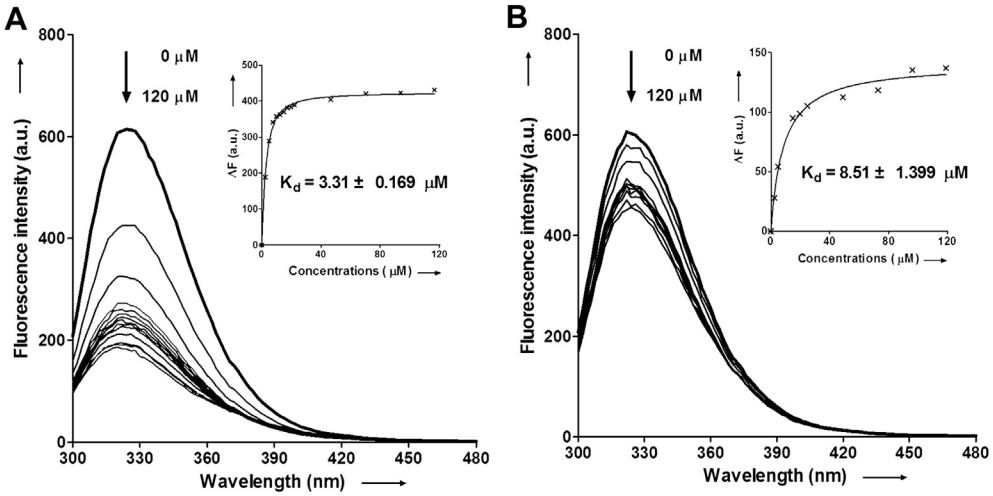

Fig. 8. Fluorescence spectra of OfHex2 (0.32 mg) in the presence of different concentrations (0–120 μM) of **20** (A) and **17** (B). In the inserted figure, the fluorescence changes at 322 nm are plotted against the inhibitor concentration.

the W441 and W478 and hydrogen bonds with H285, D344 and E345 by oxygen atom on the imide ring (Fig. 7B). And the oxygen in the linker improved the affinity of **20** by forming a hydrogen bond with the side chain of residue E345 in a distance of 2.8 Å.

Tryptophan fluorescence titration data also supported that the competitive activity of **20** benefited from the stacking interactions between naphthalimide and tryptophans. OfHex2 had a strong fluorescence emission band at around 330 nm by fixing the excitation wavelength at 280 nm (Fig. 8A). However, under the same condition, **20** had no fluorescence band but had an absorbance spectra ranging from 300 to 370 nm instead, making it a suitable potential quencher for tryptophan fluorescence. Since tryptophan residues comprised the hydrophobic wall of the active pocket [2], the interaction between **20** and the active pocket would result in the fluorescence quench of tryptophans.

As expected, by adding **20** to OfHex2, the fluorescence intensity of OfHex2 decreased in a compound-concentration dependent manner (Fig. 8A). The degrees of fluorescence quenching of OfHex2 were plotted versus the concentration of **20** (Fig. 8A, the inserted figure), and a K_d value (dissociation constant) was calculated to be 3.31 ± 0.169 μM. This confirmed the interactions between **20** and tryptophan residues at the active pocket. The same conclusion was true for **17** (Fig. 8B), which exhibited much lower inhibitory activity and weaker fluorescent quenching ability than **20**.

As shown in Fig. 9, the hydrophobic interaction between the phenyl group and the out-pocket residue H285 was strengthened, when the number of atoms between the secondary amine and phenyl fragment increased from one to three. This improvement benefited from both the length and flexibility of the linker and was consistent with inhibitory activity data. The hydrophobic group on the 4-position of the phenyl group of **13** will hurt the binding, resulting in the inhibitory activity loss of **15** and **16**.

Thus, a model of naphthalimide derivatives binding to OfHex2 was established: naphthalimide group bound to the active pocket by stacking with the tryptophan residues, the secondary amine in the flexible linker formed hydrogen bonds with the side chain of residue E345, and the small aromatic group was stacked with the H285 that located at a hydrophobic patch outside of the active pocket.

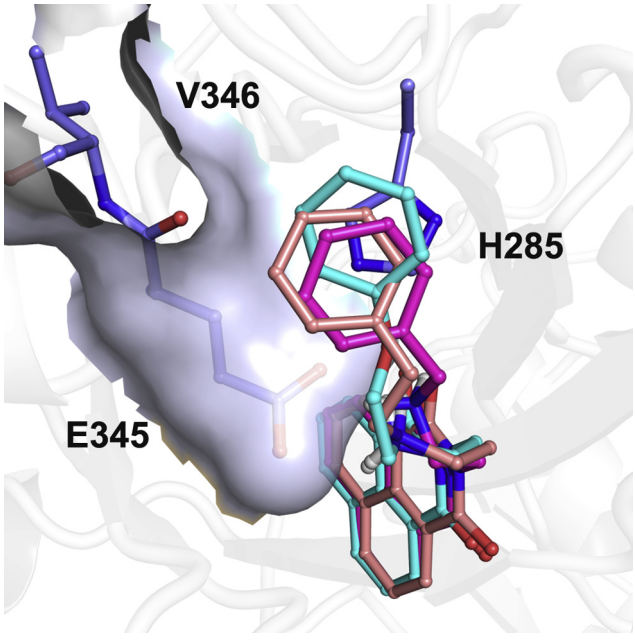

Fig. 9. Comparison of the binding model of **20** and its analogs **13** and **18**. Residues H285, E345 and V346 were shown in slate sticks. **13**, **18** and **20** were shown in magenta, salmon and cyan stick, respectively.

4. Conclusion

In conclusion, by analyzing the structure of the catalytic domain of the insect enzyme OfHex2, we designed and synthesized a series of novel naphthalimide-scaffolded compounds. The efficiency evaluation by enzymatic testing suggested most of these unsymmetrical dyads exhibited high binding efficiency and competitive inhibitory activities. The structure–activity relationship and docking studies provided a binding model between inhibitors and OfHex2. And tryptophan fluorescent assay supported that the competitive inhibition was introduced by stacking interactions between naphthalimides and tryptophans. This work provides an alternative for developing insecticides as well as inhibitors against GH20 β-*N*-acetyl-D-hexosaminidases.

Acknowledgments

This work was supported by the National High Technology Research and Development Program of China (2011AA10A204), the National Key Project for Basic Research (2010CB126100), the National Key Technology R&D Program (2011BAE06B05), the National Natural Science Foundation of China (21236002, 31070715, 31101671), the Fundamental Research Funds for the Central Universities (DUT11RC(3)73).

References

[1] J. Intra, G. Pavesi, D.S. Horner, Phylogenetic analyses suggest multiple changes of substrate specificity within the glycosyl hydrolase 20 family, BMC Evol. Biol. 8 (2008) 214. http://link.springer.com/article/10.1186%2F1471-2148-8-214.
[2] F. Liu, T. Liu, M. Qu, Q. Yang, Molecular and biochemical characterization of a novel β-*N*-acetyl-D-hexosaminidase with broad substrate-spectrum from the Asian corn borer, *Ostrinia furnacalis*, Int. J. Biol. Sci. 8 (2012) 1085–1096.
[3] F. Liu, Q. Yang, Investigation of β-N-acetyl-D-hexosaminidase as a potential target with RNA interference in Ostrinia furnacalis, Chin. J. Pestic. Sci. 15 (2013) 145–152.
[4] T. Liu, F. Liu, Q. Yang, Jun Yang, Expression, purification and characterization of the chitinolytic β-*N*-acetyl-D-hexosaminidase from the insect *Ostrinia furnacalis*, Protein Expr. Purif. 68 (2009) 99–103.
[5] T. Liu, H. Zhang, F. Liu, Q. Wu, X. Shen, Q. Yang, Structural determinants of an insect beta-*N*-Acetyl-D-hexosaminidase specialized as a chitinolytic enzyme, J. Biol. Chem. 286 (2011) 4049–4058.
[6] T. Liu, J. Yan, Q. Yang, Comparative biochemistry of GH3, GH20 and GH84 β-*N*-acetyl-D-hexosaminidases and recent progress in selective inhibitor discovery, Curr. Drug Targets 13 (2012) 512–525.
[7] T. Sumida, K.A. Stubbs, M. Ito, S. Yokoyama, Gaining insight into the inhibition of glycoside hydrolase family 20 exo-β-*N*-acetylhexosaminidases using a structural approach, Org. Biomol. Chem. 10 (2012) 2607–2612.
[8] M. Terinek, A. Vasella, Synthesis of *N*-acetylglucosamine-derived nagstatin analogues and their evaluation as glycosidase inhibitors, Helv. Chim. Acta 88 (2005) 10–22.
[9] H.C. Dorfmueller, V.S. Borodkin, M. Schimpl, S.M. Shepherd, N.A. Shpiro, D.M. van Aalten, GlcNAcstatin: a picomolar, selective O-GlcNAcase inhibitor that modulates intracellular O-GlcNAcylation levels, J. Am. Chem. Soc. 128 (2005) 16484–16485.
[10] A.F. Glawar, D. Best, B.J. Ayers, S. Miyauchi, S. Nakagawa, M. Aguilar-Moncayo, J.M. García Fernández, C. Ortiz Mellet, E.V. Crabtree, T.D. Butters, F.X. Wilson, A. Kato, G.W. Fleet, Scalable syntheses of both enantiomers of DNJNAc and DGJNAc from glucuronolactone: the effect of *N*-alkylation on hexosaminidase inhibition, Chemistry 18 (2012) 9341–9359.
[11] M.B. Tropak, S.P. Reid, M. Guiral, S.G. Withers, D. Mahuran, Pharmacological enhancement of beta-hexosaminidase activity in fibroblasts from adult Tay-Sachs and Sandhoff Patients, J. Biol. Chem. 279 (2004) 13478–13487.
[12] D.B. Langley, D.W. Harty, N.A. Jacques, N. Hunter, J.M. Guss, C.A. Collyer, Structure of *N*-acetyl-beta-D-glucosaminidase (GcnA) from the endocarditis pathogen *Streptococcus gordonii* and its complex with the mechanism-based inhibitor NAG-thiazoline, J. Mol. Biol. 377 (2008) 104–116.
[13] Y. You, T. Liu, Y. Yang, Q. Wu, Q. Yang, B. Yu, Synthesis, evaluation, and mechanism of *N*, *N*, *N*-trimethyl-D-glucosamine-(1 → 4)-chitooligosaccharides as selective inhibitors of glycosyl hydrolase family 20 β-*N*-acetyl-D-hexosaminidases, ChemBioChem 12 (2011) 457–467.
[14] H. Usuki, Y. Yamamoto, Y. Kumagai, T. Nitoda, H. Kanzaki, T. Hatanaka, MS/MS fragmentation-guided search of TMG-chitooligomycins and their structure-activity relationship in specific β-*N*-acetylglucosaminidase inhibition, Org. Biomol. Chem. 9 (2011) 2943–2951.

[15] M. Horsch, L. Hoesch, A. Vasella, D.M. Rast, *N*-acetylglucosaminono-1,5-lactone oxime and the corresponding (phenylcarbamoyl)oxime. Novel and potent inhibitors of beta-*N*-acetylglucosaminidase, Eur. J. Biochem. 197 (1991) 815–818.
[16] B. Shanmugasundaram, A.W. Debowski, R.J. Dennis, G.J. Davies, D.J. Vocadlo, A. Vasella, Inhibition of O-GlcNAcase by a gluco-conFig.d nagstatin and a PUGNAc-imidazole hybrid inhibitor, Chem. Commun. 42 (2006) 4372–4374.
[17] A. de la Fuente, R. Martin, T. Mena-Barragán, X. Verdaguer, J.M. García Fernández, C. Ortiz Mellet, A. Riera, Stereoselective synthesis of 2-Acetamido-1,2-dideoxyallonojirimycin (DAJNAc), a new potent hexosaminidase inhibitor, Org. Lett. 15 (2013) 3638–3641.
[18] C.W. Ho, S.D. Popat, T.W. Liu, K.C. Tsai, M.J. Ho, W.H. Chen, A.S. Yang, C.H. Lin, Development of GlcNAc-inspired iminocyclitiols as potent and selective *N*-acetyl-beta-hexosaminidase inhibitors, ACS Chem. Biol. 5 (2010) 489–497.
[19] M.B. Tropak, D. Mahuran, Lending a helping hand, screening chemical libraries for compounds that enhance beta-hexosaminidase A activity in GM2 gangliosidosis cells, FEBS J. 274 (2007) 4951–4961.
[20] H.C. Dorfmueller, D.M.F. van Aalten, Screening-based discovery of drug-like O-GlcNAcase inhibitor scaffolds, FEBS Lett. 584 (2010) 694–700.
[21] A. Kamal, N.R. Bolla, P.S. Srikanth, A.K. Srivastava, Naphthalimide derivatives with therapeutic characteristics: a patent review, Expert. Opin. Ther. Pat. 23 (2013) 299–317.
[22] S. Banerjee, E.B. Veale, C.M. Phelan, S.A. Murphy, G.M. Tocci, L.J. Gillespie, D.O. Frimannsson, J.M. Kelly, T. Gunnlaugsson, Recent advances in the development of 1,8-naphthalimide based DNA targeting binders, anticancer and fluorescent cellular imaging agents, Chem. Soc. Rev. 42 (2013) 1601–1618.
[23] M.B. Tropak, J.E. Blanchard, S.G. Withers, E.D. Brown, D. Mahuran, High-throughput screening for human lysosomal beta-*N*-Acetyl hexosaminidase inhibitors acting as pharmacological chaperones, Chem. Biol. 14 (2007) 153–164.
[24] P. Guo, Q. Chen, T. Liu, L. Xu, Q. Yang, X.H. Qian, Development of unsymmetrical dyads as potent noncarbohydrate-based inhibitors against human beta-*N*-Acetyl-D-hexosaminidase, ACS Med. Chem. Lett. 4 (2013) 527–531.
[25] A.L. Hopkins, C.R. Groom, A. Alex, Ligand efficiency: a useful metric for lead selection, Drug Discov. Today 9 (2004) 430–431.
[26] I. Ott, Y. Xu, X. Qian, Fluorescence properties and antiproliferative effects of *mono*-, *bis*-, and *tris*- thiophenylnaphthalimides: results of a comparative pilot study, J. Photochem. Photobiol. B 105 (2011) 75–80.
[27] T. Liu, H. Zhang, F. Liu, L. Chen, X. Shen, Q. Yang, Active-pocket size differentiating insectile from bacterial chitinolytic β-*N*-acetyl-D-hexosaminidases, Biochem. J. 438 (2011) 467–474.
[28] M.G.J. Baud, P. Haus, T. Leiser, F.J. Meyer-Almes, M.J. Fuchter, Highly ligand efficient and selective N-2-(Thioethyl)picolinamide histone deacetylase inhibitors inspired by the natural product psammaplin A, ChemMedChem 8 (2013) 149–156.
[29] K. Arnold, L. Bordoli, J. Kopp, T. Schwede, The SWISS-MODEL workspace: a web-based environment for protein structure homology modelling, Bioinformatics 22 (2006) 195–201.
[30] P. Benkert, M. Biasini, T. Schwede, Toward the estimation of the absolute quality of individual protein structure models, Bioinformatics 27 (2011) 343–350.
[31] D.M. van Aalten, R. Bywater, J.B. Findlay, M. Hendlich, R.W. Hooft, G. Vriend, PRODRG, a program for generating molecular topologies and unique molecular descriptors from coordinates of small molecules, J. Comput. Aided Mol. Des. 10 (1996) 255–262.
[32] A.W. Schüttelkopf, D.M. van Aalten, Acta. PRODRG: a tool for high-throughput crystallography of protein-ligand complexes, Crystallogr. D Biol. Crystallogr. 60 (2004) 1355–1363.
[33] G.M. Morris, D.S. Goodsell, R.S. Halliday, R. Huey, W.E. Hart, R.K. Belew, A.J. Olson, Automated docking using a lamarckian genetic algorithm and empirical binding free energy function, J. Comput. Chem. 19 (1998) 1639–1662.
[34] G.M. Morris, R. Huey, W. Lindstrom, M.F. Sanner, R.K. Belew, D.S. Goodsell, A.J. Olson, AutoDock4 and AutoDockTools4: automated docking with selective receptor flexibility, J. Comput. Chem. 30 (2009) 2785–2791.
[35] W.C. Chao, J.F. Lu, J.S. Wang, H.C. Yang, T.A. Pan, S.C. Chou, L.H. Wang, P.T. Chou, Probing ligand binding to thromboxane synthase, Biochemistry 52 (2013) 1113–1121.
[36] Y. Jiang, W. Yu, J. Zhang, C. Frolet, A. Di Guilmi, C. Zhou, T. Vernet, Y. Chen, Structural basis for the substrate specificity of a novel β-*N*-acetylhexosaminidase StrH protein from Streptococcus pneumoniae R6, J. Biol. Chem. 286 (2011) 43004–43012.
[37] K.S. Bateman, M.M. Cherney, D.J. Mahuran, M. Tropak, M.N. James, Crystal structure of β-hexosaminidase B in complex with pyrimethamine, a potential pharmacological chaperone, J. Med. Chem. 54 (2011) 1421–1429.
[38] Y. Wang, T. Liu, Q. Yang, Z. Li, X.H. Qian, A modeling study for structure features of β-*N*-acetyl-D-hexosaminidase from Ostrinia furnacalis and its novel inhibitor allosamidin: species selectivity and multi-target characteristics, Chem. Biol. Drug Des. 79 (2012) 572–582.